Electronic Supplementary Information (ESI)

Lanthanide-based metal-organic framework materials as bifunctional fluorescence sensors toward acetylacetone and aspartic acid

Yu-Guang Li, Jun-Jie Hu, Jia-Li Zhang, Sui-Jun Liu,* Yan Peng and He-Rui Wen*

School of Chemistry and Chemical Engineering, Jiangxi Provincial Key Laboratory of Functional Molecular Materials Chemistry, Jiangxi University of Science and Technology, Ganzhou 341000, Jiangxi Province, P.R. China

*Corresponding authors. E-mail: sjliu@jxust.edu.cn (S.-J. Liu), wenherui63@163.com (H.-R. Wen). Tel: +86-797-8312289, +86-797-8312204.

Table S1. Selected bond lengths (Å) and angles (°) for **Gd-MOF 1**.

O285—Gd03^{i}	2.284(6)	O10—Gd05	2.274(6)
O17—Gd01^{ii}	2.381(5)	O267—Gd01^{vi}	2.388(5)
O9—Gd05^{iii}	2.251(6)	O141—Gd05^{vii}	2.296(6)
O60—Gd01^{iv}	2.508(5)	O141—Gd03^{vii}	2.783(6)
O61—Gd01^{iv}	2.429(5)	O142—Gd03^{vii}	2.460(6)
C48—Gd01^{iv}	2.831(7)	C138—Gd03^{vii}	3.013(8)
O16—Gd01^{v}	2.271(6)	O57—Gd02^{viii}	2.442(5)
O58—Gd02^{viii}	2.589(6)	C54—Gd02^{viii}	2.883(7)
O278—Gd01^{iv}	2.322(6)	O11—Gd05^{vii}	2.360(5)
Gd01—O305	2.458(5)	O1—Gd04	2.487(6)
Gd01—O303	2.636(6)	Gd02—O14	2.308(6)
Gd01—C297	2.911(8)	Gd02—O165^{iii}	2.385(5)
Gd02—O246^{ix}	2.408(5)	Gd02—O15	2.391(6)
Gd02—O295^{iii}	2.526(5)	Gd02—O254^{iii}	2.403(5)
Gd02—O13^{ix}	2.765(6)	Gd03—O248^{i}	2.340(6)
Gd02—C253^{iii}	2.842(7)	Gd03—O283^{iii}	2.396(6)
Gd02—C143^{ix}	2.932(8)	Gd03—O259	2.440(6)
Gd03—O284^{iii}	2.560(6)	Gd04—O300^{x}	2.248(6)
Gd03—C258	2.811(7)	Gd04—O80	2.286(6)
Gd03—C244^{iii}	2.811(9)	Gd04—O287^{ix}	2.354(6)
Gd03—O237	2.495(6)	Gd03—O12	2.484(5)
Gd04—O13	2.370(6)	Gd03—O284^{iii}	2.560(6)
Gd04—O164^{vii}	2.439(5)	Gd04—C161^{vii}	2.886(7)
Gd04—O147	2.439(6)	Gd05—O247^{i}	2.350(6)
Gd04—O165^{vii}	2.573(5)	Gd05—O274	2.419(5)
Gd04—C199	2.810(9)	Gd05—O237	2.533(5)
Gd05—C269	2.827(7)		
O248^{i}-Gd03-O285^{i}	81.57(256)	O58^{v}-Gd02-O254^{iii}	71.47(217)
O285^{i}-Gd03-O12	80.15(245)	O14-Gd02-O295^{iii}	81.15(211)
O237-Gd03-O142^{xi}	116.91(201)	O15-Gd02-O165^{iii}	85.21(226)
O259-Gd03-O284^{iii}	72.03(234)	O13^{ix}-Gd02-O246^{ix}	49.71(193)
O12-Gd03-O285^{i}	80.13(215)	O57^{v}-Gd02-O246^{ix}	89.58(269)
O305-Gd01-O278^{iv}	70.09(222)	O80-Gd04-O1	82.41(245)
O267^{vi}-Gd01-O17^{ix}	81.80(228)	O147-Gd04-O300^{x}	77.69(248)
O16^{vii}-Gd01-O60^{iv}	83.55(239)	O13-Gd04-O165^{viii}	70.23(164)
O303^{iv}-Gd01-O61	74.02(201)	O164^{viii}-Gd04-O287^{ix}	74.99(217)
O9^{iii}-Gd05-O10	95.39(261)	O237-Gd05-O141^{xi}	75.66(210)
O11^{xi}-Gd05-O247^{i}	78.55(247)	O274-Gd05-O9^{iii}	77.67(246)

Symmetry codes: (i) -*x*+2, -*y*+1, -*z*+1; (ii) *x*-1, *y*, *z*-1; (iii) -*x*+1, -*y*+1, -*z*+1; (iv) -*x*+2, -*y*, -*z*+2; (v) *x*-1, *y*, *z*; (vi) -*x*+2, -*y*+1, -*z*+2; (vii) *x*, *y*-1, *z*; (viii) *x*+1, *y*, *z*; (ix) -*x*+1, -*y*, -*z*+1; (x) -*x*+2, -*y*, -*z*+1; (xi) *x*, *y*+1, *z*.

Table S2. SHAPE analysis of the Gd^{III} ion in **Gd-MOF 1**.

Complex	Metal Ions	Label	Shape	Symmetry	Distortion(τ)
Gd-MOF 1	Gd05	HP-7	D_{7h}	Heptagon	33.900
		HPY-7	C_{6v}	Hexagonal pyramid	22.417
		PBPY-7	D_{5h}	Pentagonal bipyramid	2.957
		COC-7	C_{3v}	Capped octahedron	3.509
		CTPR-7	$\boldsymbol{C_{2v}}$	**Capped trigonal prism**	**2.619**
		JPBPY-7	D_{5h}	Johnson pentagonal bipyramid J13	6.185
		JETPY-7	C_{3v}	Johnson elongated triangular pyramid J7	20.340
	Gd01/Gd04	OP-8	D_{8h}	Octagon	30.872/29.067
		HPY-8	C_{7v}	Heptagonal pyramid	23.104/24.280
		HBPY-8	D_{6h}	Hexagonal bipyramid	12.953/11.468
		CU-8	O_h	Cube	11.945/9.576
		SAPR-8	D_{4d}	Square antiprism	4.414/4.577
		TDD-8	D_{2d}	Triangular dodecahedron	3.227/3.672
		JGBF-8	D_{2d}	Johnson gyrobifastigium J26	11.467/9.366
		JETBPY-8	D_{3h}	Johnson elongated triangular bipyramid J14	25.524/24.302
		JBTPR-8	C_{2v}	Biaugmented trigonal prism J50	3.462/3.713
		BTPR-8	$\boldsymbol{C_{2v}}$	**Biaugmented trigonal prism**	**3.115**/3.202
		JSD-8	$\boldsymbol{D_{2d}}$	**Snub diphenoid J84**	3.734/**3.136**
		TT-8	T_d	Triakis tetrahedron	12.520/10.346
		ETBPY-8	D_{3h}	Elongated trigonal bipyramid	22.991/21.913
	Gd02/Gd03	EP-9	D_{9h}	Enneagon	32.964/33.640
		OPY-9	C_{8v}	Octagonal pyramid	22.185/22.096
		HBPY-9	D_{7h}	Heptagonal bipyramid	17.458/17.820
		JTC-9	C_{3v}	Johnson triangular cupola J3	14.219/14.982
		JCCU-9	C_{4v}	Capped cube J8	7.798/10.333
		CCU-9	C_{4v}	Spherical-relaxed capped cube	6.638/8.874
		JCSAPR-9	C_{4v}	Capped square antiprism J10	3.782/3.973
		CSAPR-9	C_{4v}	Spherical capped square antiprism	2.911/2.887
		JTCTPR-9	D_{3h}	Tricapped trigonal prism J51	3.895/4.963
		TCTPR-9	D_{3h}	Spherical tricapped trigonal prism	3.908/3.547
		JTDIC-9	C_{3v}	Tridiminished icosahedron J63	12.277/11.861
		HH-9	C_{2v}	Hula-hoop	8.119/8.382
		MFF-9	$\boldsymbol{C_s}$	**Muffin**	**2.181/2.350**

Table S3. Comparison of the sensitivities of **Tb-MOF 2** with previously reported MOFs to acac and Asp.

analytes	MOFs	solvents	detection	references

			limits (ppm)	
acac	**Tb-MOF 2**	EtOH	0.129	This work
	$[Zn_3(BIBT)(BTC)_{5/3}(\mu_3\text{-}OH)]\cdot solvents\}_n$	DMAc	17.36	1
	$[Cd_2(TFBA)(HCOO)(bpe)H_2O]_n$	DMF	37.3	2
	$[Cd(HL1)(bpy)]\cdot 1.25H_2O\cdot 1.5DMF\}_n$	DMF	0.136	3
	Tb-MOF	$MeOH/H_2O$=1:1	144	4
	$\{[Zn_2(XN)_2(IPA)_2]\cdot 2H_2O\}_n$	DMF	0.250	5
Asp	**Tb-MOF 2**	EtOH	0.025	This work
	Eu-MOF	H_2O	0.378	6
	$\{[(Me_2NH_2)_2][Cd_2K_2(L2)_2(H_2O)]\}_n$	H_2O	0.428	7
	Ag^+@Eu-complex	H_2O	0.079	8
	Cu/Tb@Zn-MOF	H_2O	0.540	9
	$\{Eu_{0.4}[Ni_2(odip)(H_2O)_4(DMF)](NO_3)_{1.2}\cdot 0.5DMF\cdot H_2O\}_n$	DMF/H_2O = 2:1	0.429	10

H_3L1 = 5-(4-carboxybenzylamino)isophthalic acid

bpy = 4,4′-bipyridine

BIBT = 4,7-bi(1Himidazol-1-yl)benzo-[2,1,3]thiadiazole

H_3BTC = 1,3,5-benzenetricarboxylic acid

H_3TFBA = tris(3′-F-4′-carboxybiphenyl)amine

bpe = trans-1,2-bis(4-pyridyl)ethene

XN = 4′-(4-pyridine)4,2′:2′,4″-terpyridine

IPA = isophthalic acid

H_4L2 = terphenyl-2, 2′, 4, 4′-tetracarboxylic acid

H_4odip = 5,5′-oxidiisophthalic acid;

References

1. L. Q. Li, S. L. Yao, X. M. Tian, T. F. Zheng, J. Y. Li, S. J. Liu, J. L. Chen, M. H. Yu and H. R. Wen, *CrystEngComm*., **2021**, 23, 2532−2537.

2. J. Ru, R. F. Zhang, X. Y. Li, Y. X. Wang, L. L. Li and C. L. Ma, *J. Solid State Chem*., **2022**, 307, 122820.

3. Y. Yu, Y. Wang, H. Xu, J. Lu, H. Wang, D. Li, J. Dou, Y. Li and S. Wang, *CrystEngComm*., **2020**, 22, 3759−376.

4. J. X. Li, B. Q. Yu, L.H. Fan, L. Wang, Y. C. Zhao, C. Y. Sun, W. J. Li and Z. D. Chang, *J. Solid State Chem*., **2022**, 306, 122782.

5. X. M. Kang, X. Y. Fan, P. Y. Hao, W. M. Wang and B. Zhao, *Inorg. Chem. Front.*, **2019**, 6, 271−277.

6. Y. X. Sun, G. Guo, W. M. Ding, W. Y. Han, J. Li and Z. P. Deng, *CrystEngComm.*, **2022**, 24, 1358−1367.

7. L. B. Wang, J. J. Wang, E. L. Yue, L. Tang, X. Wang, X. Y. Hou, Y. Zhang, Y. X. Ren and X. L. *Spectrochim. Acta, Part A*, 2022, 265, 120340.

8. H. Weng and B. Yan, *Sens. Actuators, B*, **2017**, 253, 1006−1011.

9. G. Ji, T. Zheng, X. Gao and Z. Liu, *Sens. Actuators, B*, **2017**, 284, 91−95.

10. Y. Liu, Y. K. Lu, B. Zhang, L. Hou and Y. Y. Wang, *Inorg. Chem.*, **2020**, 59, 7531−7538.

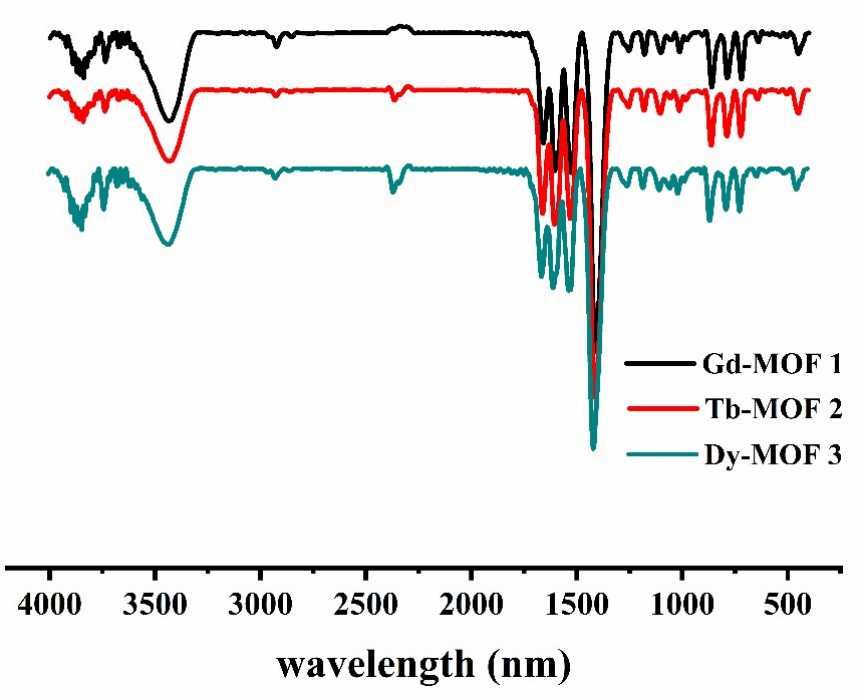

Fig. S1 IR spectra of **Ln-MOFs 1–3** at room temperature.

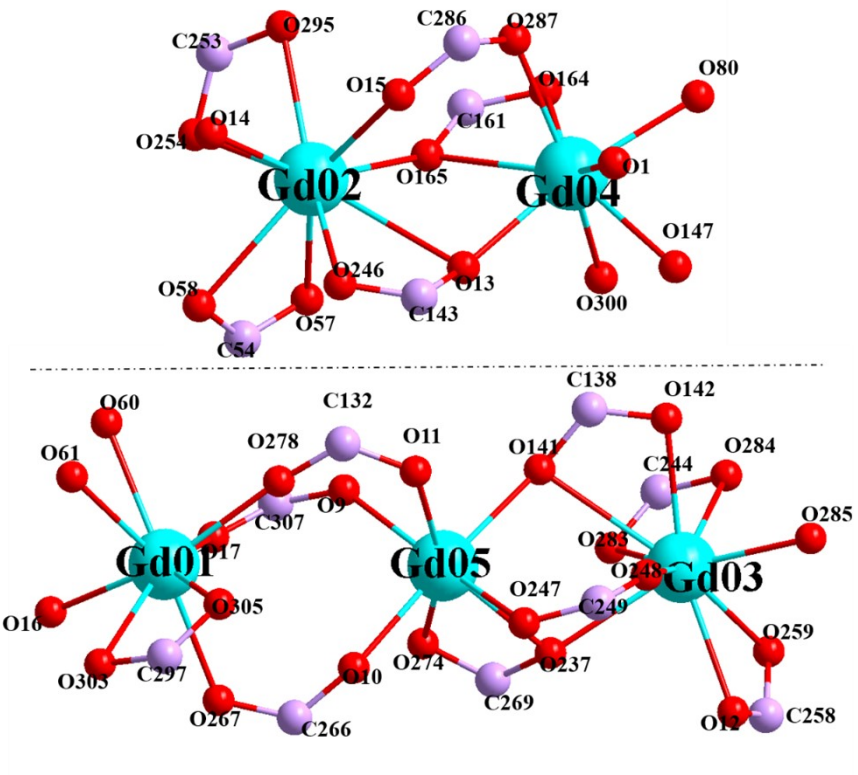

Fig. S2 Coordination environments of Gd^{III} ions in **Gd-MOF 1**.

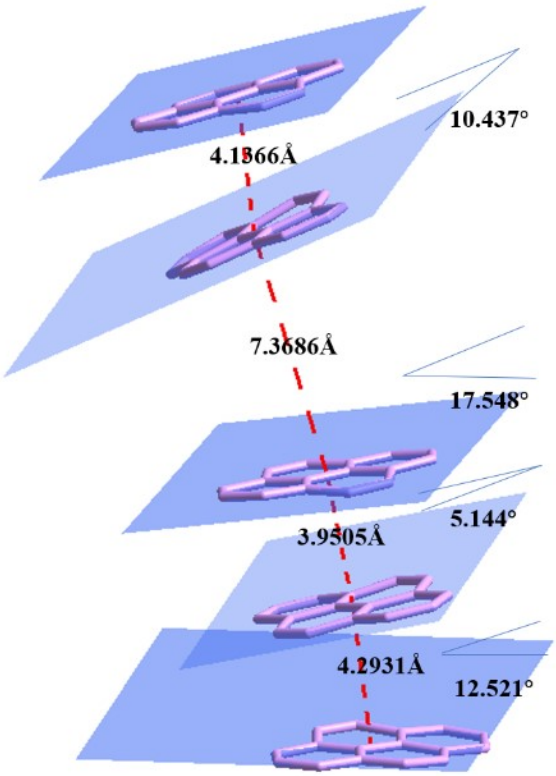

Fig. S3 The angles and distances between the adjacent layers of pyrene rings in the center of the ligand for **Gd-MOF 1**.

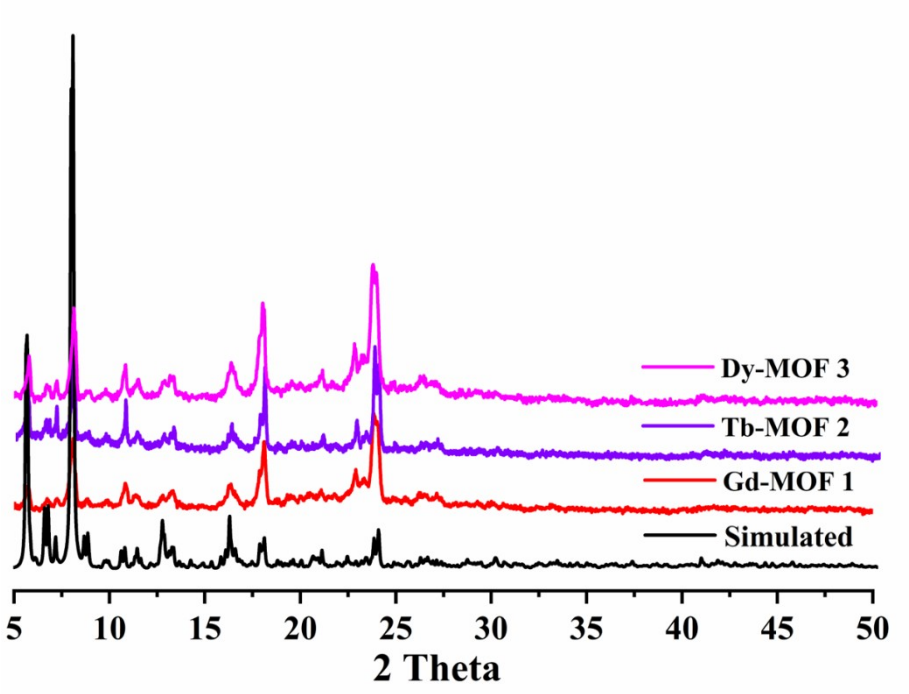

Fig. S4 The simulated and experimental PXRD patterns of **Ln-MOFs 1**–**3**.

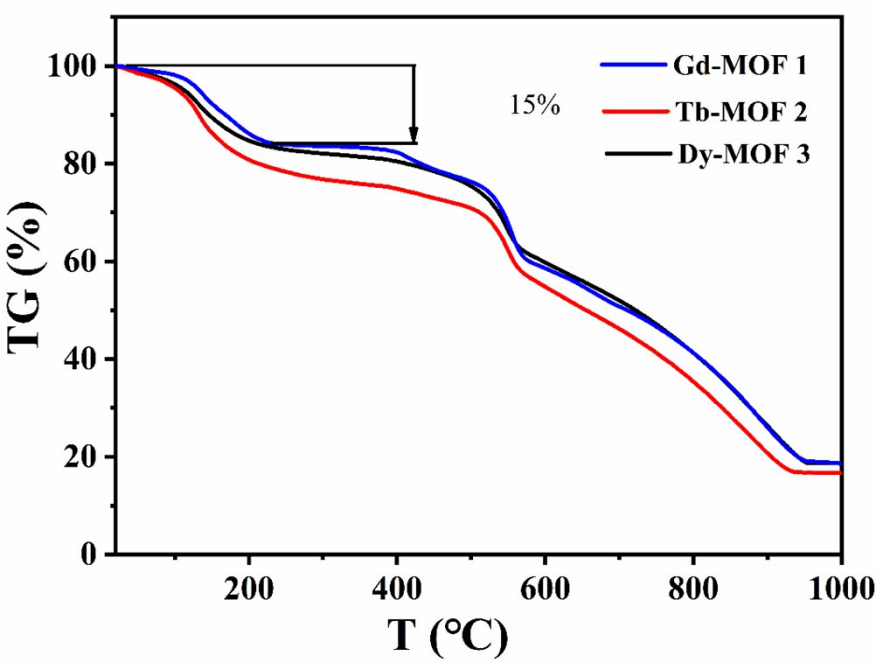

Fig. S5 The TGA curves for **Ln-MOFs 1**–**3**.

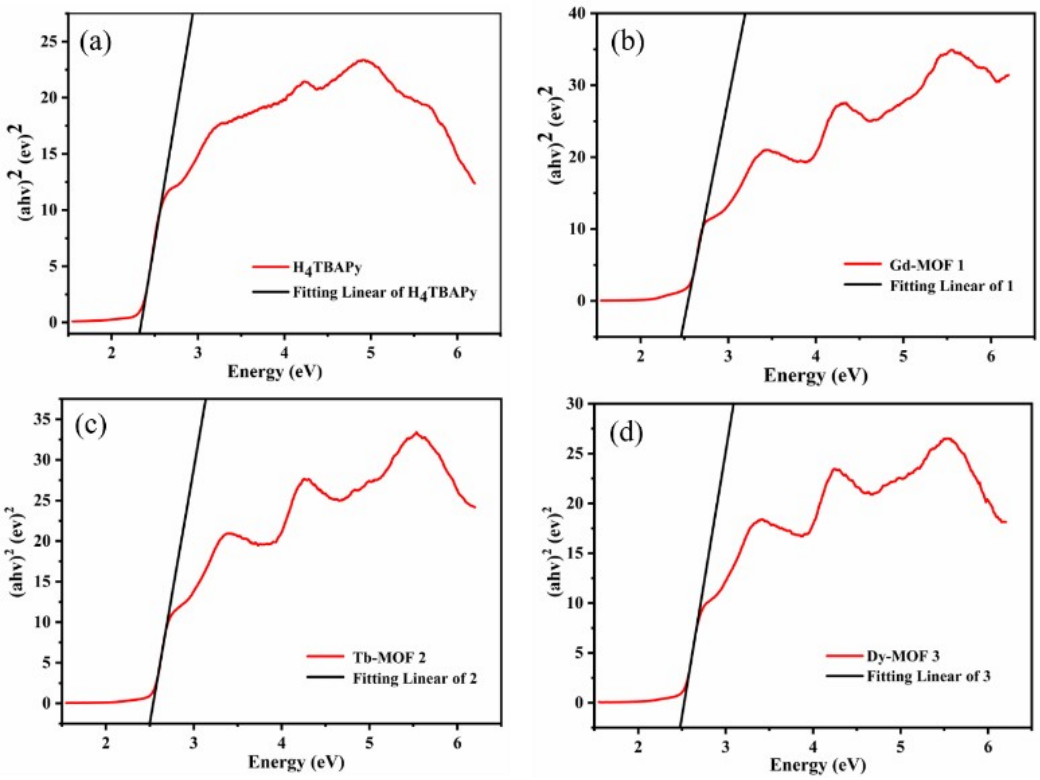

Fig. S6 The optical band gaps of H_4TBAPy and **Ln-MOFs 1–3** calculated from the UV-Vis absorption spectra.

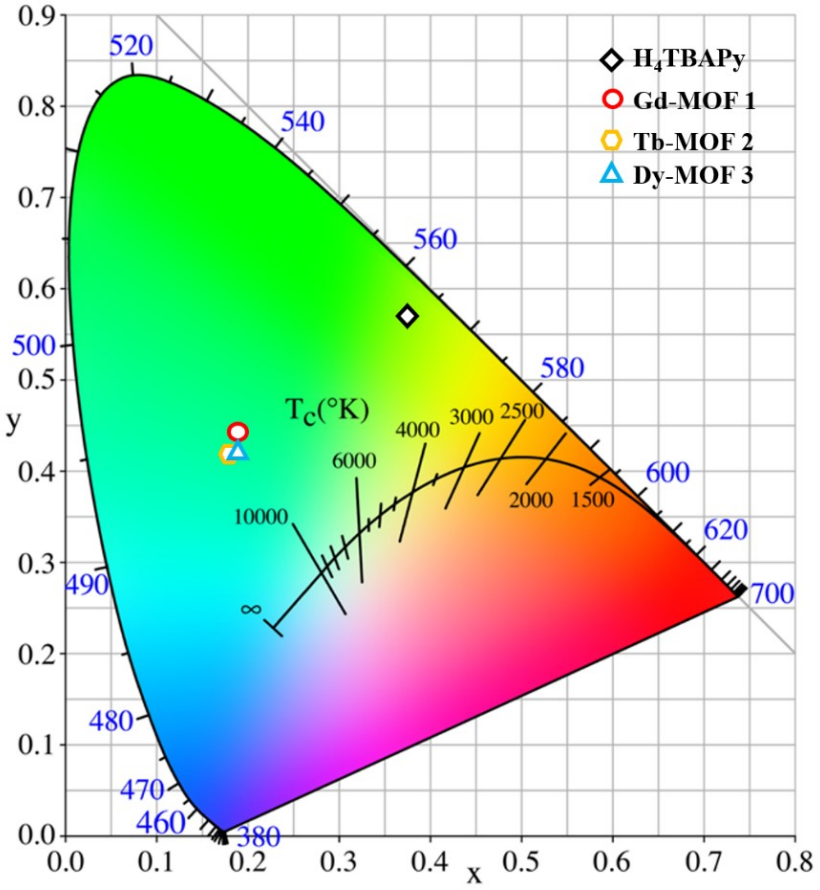

Fig. S7 CIE chromaticity diagram of H_4TBAPy and **Ln-MOFs 1–3** (λ_{ex} = 396 nm).

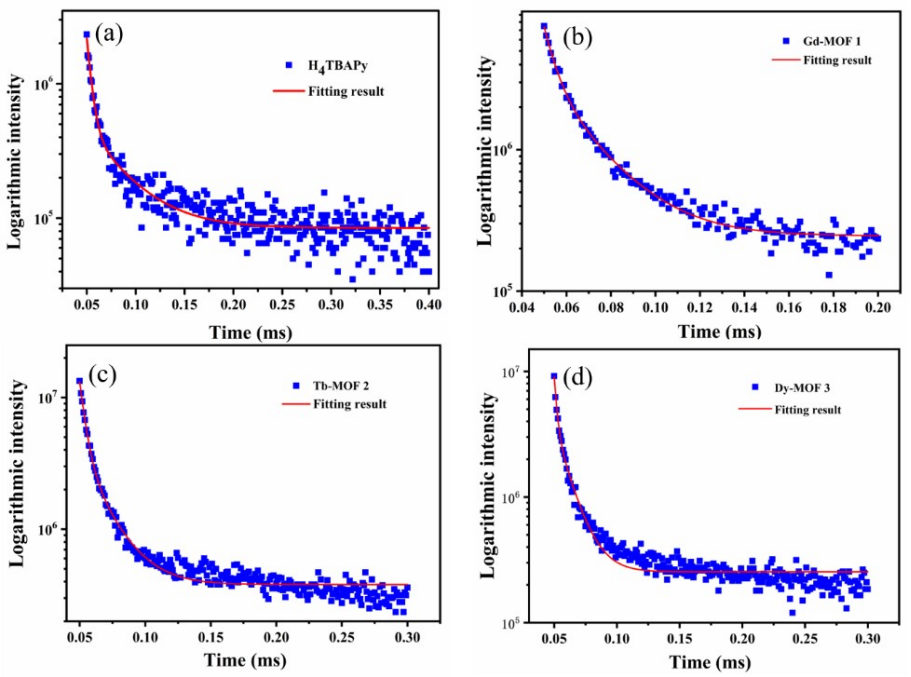

Fig. S8 Fluorescence decay curves of H_4TBAPy (a) and **Ln-MOFs 1**–**3** (b-d).

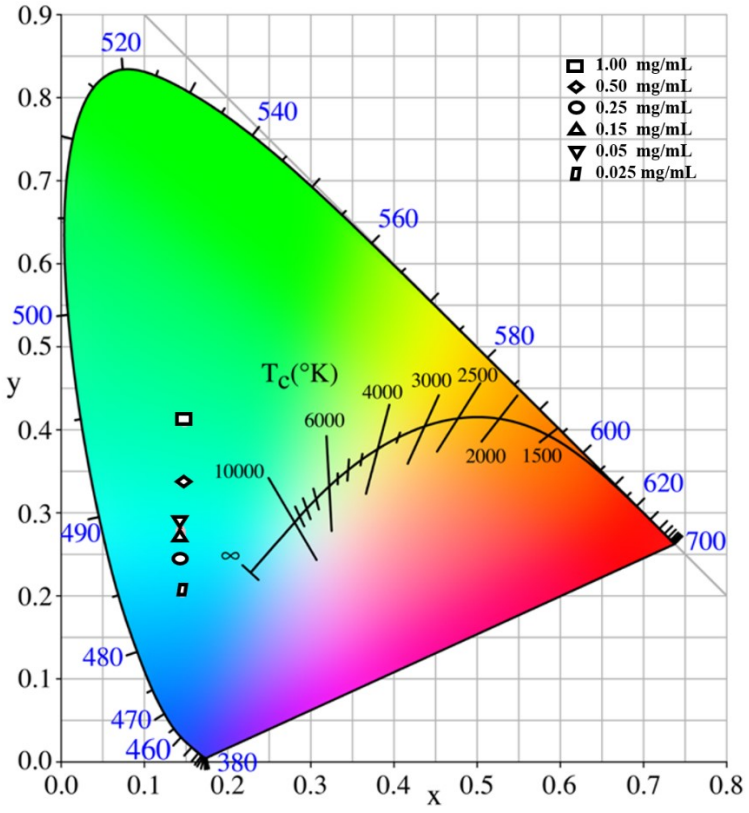

Fig. S9 CIE chromaticity diagram of **Tb-MOF 2** in different ethanol suspensions.

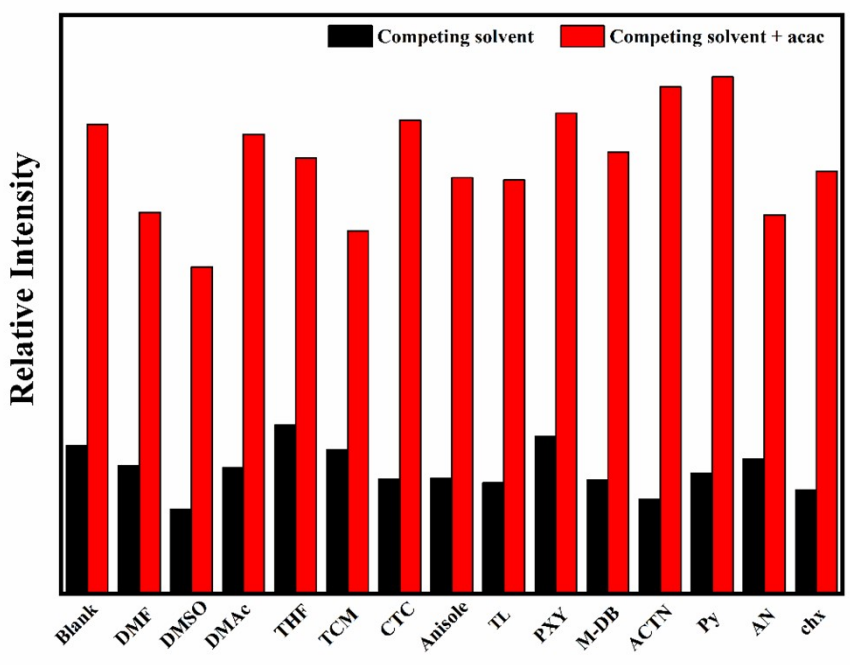

Fig. S10 Competitive experiments of **Tb-MOF 2** in sensing acac with the interference of other interfering organic solvents in ethanol solution.

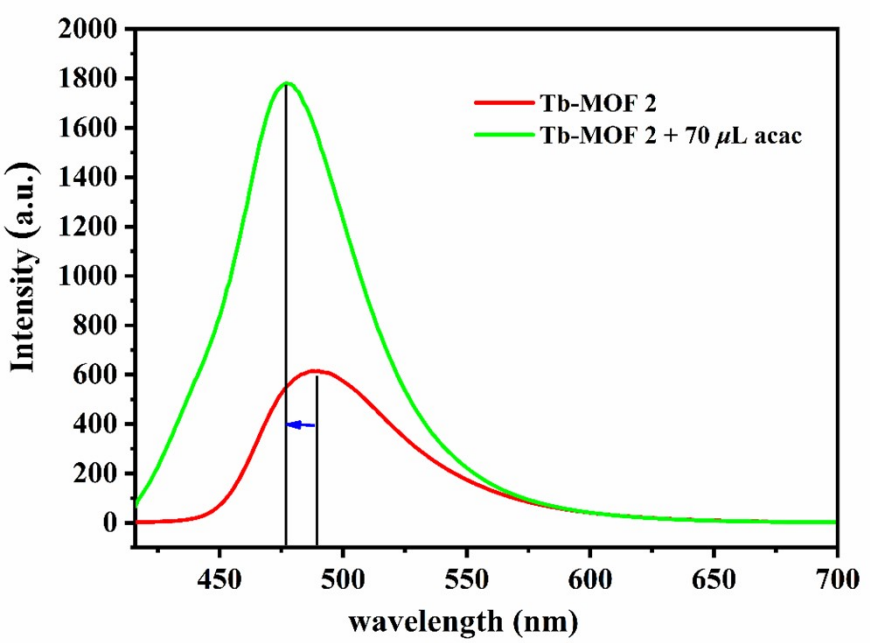

Fig. S11 Relative fluorescence intensity of **Tb-MOF 2** and **Tb-MOF 2** adding 70 μL acac in ethanol solution.

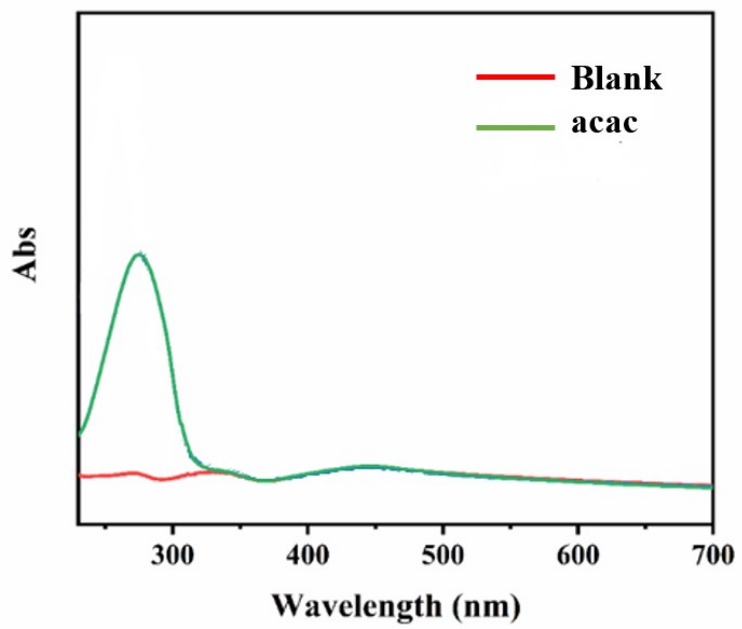

Fig. S12 UV-Vis absorption spectra of **Tb-MOF 2** and **Tb-MOF 2** upon the addition of acac.

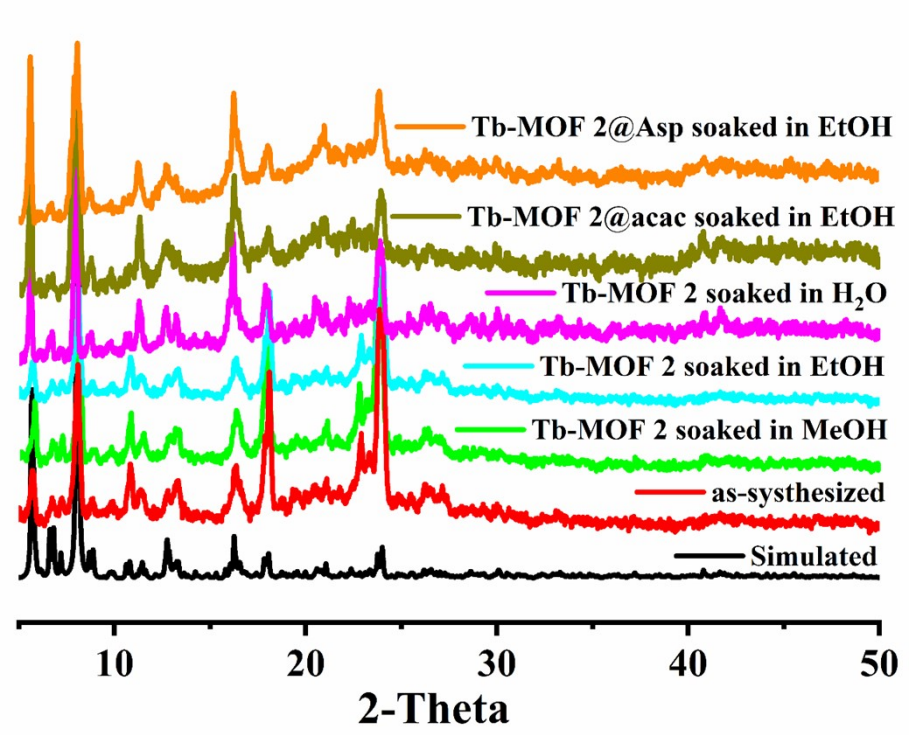

Fig. S13 The simulated and experimental PXRD patterns of **Tb-MOF 2**, **Tb-MOF 2@**acac and **Tb-MOF 2@**Asp soaked in MeOH, EtOH and aqueous solution for 12 h.

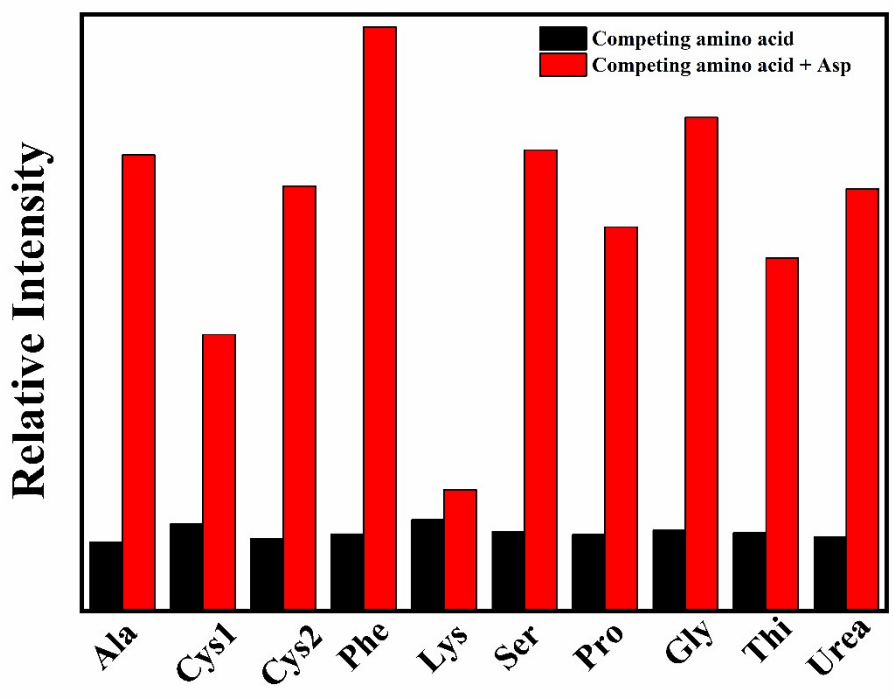

Fig. S14 Competitive experiments of **Tb-MOF 2** in sensing Asp with the interference of other amino acids in ethanol solution.

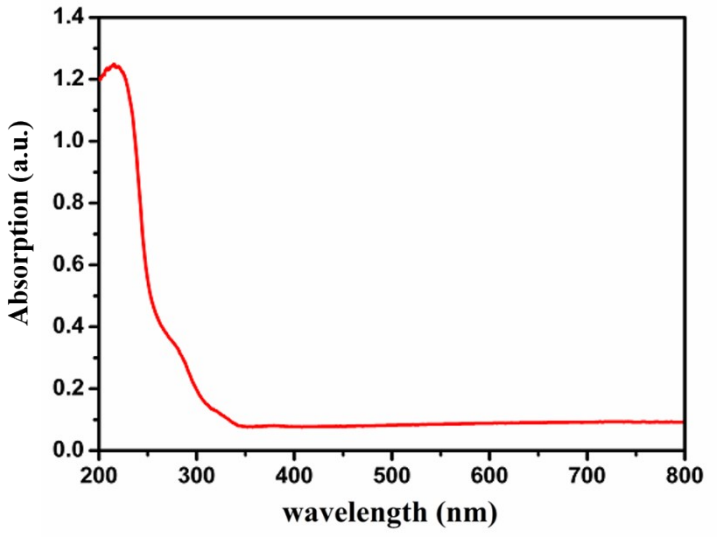

Fig. S15 Solid-state UV-Vis absorption spectrum of Asp.